JOURNAL OF GUIDANCE, CONTROL, AND DYNAMICS
Vol. 33, No. 3, May–June 2010

Reachable Domain for Spacecraft with a Single Impulse

Dan Xue,* Junfeng Li,† Hexi Baoyin,‡ and Fanghua Jiang§
Tsinghua University, 100084 Beijing, People's Republic of China

DOI: 10.2514/1.43963

This paper analyzes the reachable domain for spacecraft with a single fixed-magnitude impulse, and over-approximation of the reachable domain is provided for cases involving spacial impulse. A low impulse is assumed, implying elliptical trajectories and a bounded reachable domain. An equation is developed for the trajectory, with no restriction on the eccentricity of the initial elliptical orbit. A method is given to determine both the envelope of the ellipsoids of revolution containing the trajectories and the envelope of the planes containing the trajectories, with the intersection of these two envelopes found to be the upper bound on the reachable domain. The reachable domain is given for three scenarios for different missions, with several examples given to demonstrate the efficiency of this method.

Nomenclature

C_{EB}	=	rotation matrix for transformation from frame $Bxyz$ into frame $EXYZ$
e	=	eccentricity, $\|\boldsymbol{e}\|$
$\boldsymbol{e}$	=	eccentricity vector
h	=	angular momentum vector magnitude, $\|\boldsymbol{h}\|$
$\boldsymbol{h}$	=	angular momentum vector
p	=	semilatus rectum
R	=	magnitude of position vector of a point on the ellipsoid of revolution, $\|\boldsymbol{R}\|$
$\boldsymbol{R}$	=	position vector of a point on the ellipsoid of revolution
r	=	distance from the spacecraft to the Earth's center, $\|\boldsymbol{r}\|$
$\boldsymbol{r}$	=	position vector
s, m, n	=	variables transforming equations from trigonometric forms into parametric algebraic forms
v	=	velocity vector magnitude, $\|\boldsymbol{v}\|$
$\boldsymbol{v}$	=	velocity vector
x, y, z	=	components of position vector expressed in frame $EXYZ$
α	=	impulse azimuth
β	=	flight-path angle
γ	=	impulse elevation
$\Delta\boldsymbol{i}$	=	angle between the planes of the trajectory and the initial orbit
$\Delta\boldsymbol{v}$	=	impulse vector
θ	=	angle between the vectors for a point on the trajectory and the point of application
ι	=	position azimuth of a point on the ellipsoid of revolution
κ	=	position elevation of a point on the ellipsoid of revolution
λ	=	impulse vector magnitude
μ	=	gravitational constant
υ	=	true anomaly
ω	=	argument of perigee

Subscripts

0	=	initial orbit
1	=	trajectory

Superscripts

B	=	vector expressed in frame $Bxyz$
E	=	$EXYZ$

I. Introduction

WITH the growing number of on-orbit spacecraft, the maneuverability potential for the spacecraft with the available fuel is becoming increasingly important. On the other hand, for autonomous proximity operations, such as formation flying [1], rendezvous [2], and on-orbit servicing spacecraft [3], evaluation of the safe distance between spacecraft is quite critical because of the larger collision possibility due to the continuous proximity.

Thrust impulse is a commonly used maneuver mode to adjust an orbit, with the application of multiple thrust impulses used to accomplish any desired orbit maneuver [4]. Previous orbit maneuver research has typically been done according to specific applications. The point of application, as well as the direction and magnitude of the impulses, are determined by optimizing the trajectory, with the usual performance index being to minimize fuel consumption [5,6]. In these studies, collision avoidance is achieved by imposing safety as a constraint on the trajectory optimization or an optimization objective [7–9]. However, these methods only consider situations with prescribed maneuver objectives with the assumption that the sufficient fuel is available.

Ascertaining the reachable domain with the limited fuel potential can be used as a precondition for collision possibility analysis. Vinh et al. [10] focused on the problem of intercepting an intercontinental ballistic missile and defined the reachable surface as the boundary of the set of all attainable points at a given time. They investigated the reachable domain of an interceptor at hyperbolic speeds with a single impulse, with the boundary for short durations shown to be an ellipsoid. However, this method is only suitable for situations with time constraints. Battin [11] investigated the coplanar scope of accessibility for a space vehicle from a certain point with a fixed speed, noting that the elliptical locus is the envelope of all possible orbits. This conclusion is of theoretical importance, but the applications are limited because different spacecraft rarely reach the same location at a common speed.

Almost all intercept problems have been analyzed based on the assumption of a single-impulse mode [12]. In the same way, the entire reachable domain for the spacecraft should be evaluated based on using all the fuel to expand or shrink the orbital ellipse and rotate the orbital plane. Furthermore, there is no terminal constraint that

Received 23 February 2009; revision received 5 February 2010; accepted for publication 23 February 2010.

*Assistant Researcher, School of Aerospace; xuedan_tsinghua@126.com.
†Professor, School of Aerospace; lijunf@tsinghua.edu.cn.
‡Associate Professor, School of Aerospace; baoyin@tsinghua.edu.cn.
§Assistant Researcher, School of Aerospace; jiangfh04@mails.thu.edu.cn.

needs to be satisfied by adding extra impulses to adjust the trajectory. Therefore, the single-impulse mode is preferred to the multi-impulse mode.

This study aims at determining the reachable domain for spacecraft with a single fixed-magnitude impulse. The impulse magnitude is assumed to be small, implying that all the trajectories are ellipses and the reachable domain is bounded. The method for determining the reachable domain developed here has no restriction on the eccentricity of the initial elliptical orbit. The requirements for different space missions are taken into account with three scenarios:

1) The point of application is fixed and the impulse direction is arbitrary.

2) The point of application is arbitrary and the impulse direction is fixed.

3) Both the point of application and the impulse direction are arbitrary.

Note that the spacecraft is assumed to move in a Keplerian central gravitational field. In addition, the analysis assumes that the attitude control system of the spacecraft allows the impulse to be oriented freely and the impulse direction is constrained only as specified in the scenario.

The rest of this paper is organized as follows. First, the envelope definition is reviewed for a curve family in a plane and for a surface family. Then an equation is developed for the trajectory based on the angular momentum and eccentricity vectors, followed by the equations for the ellipsoid of revolution and the plane containing the trajectory. After that, the reachable domain for spacecraft is determined for the three scenarios, with numerical simulations for each scenario.

II. Envelope Definition

The intuitive envelope definition presented by Spivak [13] states that the envelope can generally be regarded as consisting of the intersections of members of the family with another member infinitely close to it. As shown in Fig. 1, for the case of coplanar impulse and fixed point of application, the thin real line represents the initial orbit, after impulses of variable direction are applied at the initial point, trajectories denoted with broken lines are generated, and various trajectories form the reachable domain, denoted with the shadow. The thick real lines represent the boundary of the reachable domain, which is exactly the envelope of the family of elliptical trajectories.

For a family of curves in a plane $y = f(x, \alpha)$, where α is a parameter, the envelope is defined to be a curve l, which is not a member of this family but is tangent to some member of the family at every point. The function l obeys

$$\begin{cases} y = f(x, \alpha) \\ \frac{\partial f}{\partial \alpha} = 0 \end{cases} \tag{1}$$

Analogously, for a family of surfaces $F(x, y, z, \alpha) = 0$, where α is the parameter and $\partial F/\partial x$, $\partial F/\partial y$, and $\partial F/\partial z$ are not all equal to zero, the surface-family envelope obeys

$$\begin{cases} F(x, y, z, \alpha) = 0 \\ \frac{\partial F(x,y,z,\alpha)}{\partial \alpha} = 0 \end{cases} \tag{2}$$

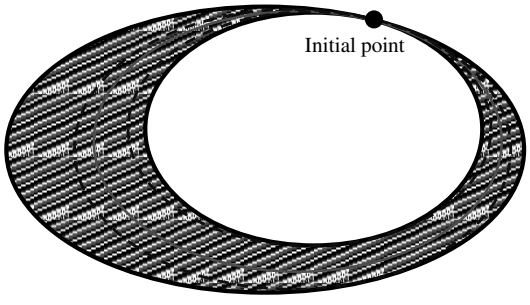

Fig. 1 Reachable domain and envelope for the coplanar impulse case.

Since a plane is a special kind of surface, the envelope definition for a surface family also fits for a family of nonparallel planes. In this case, the envelope is known to be a ruled surface; especially, a line is the envelope of a pencil of surfaces. Note that the solution of Eqs. (1) and (2) probably contain cusps that should be evaluated and possibly removed.

Similar considerations could be applied to a multiparameter family of curves in a plane as well as a multiparameter family of surfaces.

III. Equations for Trajectories

Several coordinate frames are used in the analysis.

With frame $EXYZ$, the frame's origin is at the Earth's center, the X axis points in the perigee of the initial orbit direction, the Z axis points in the cross-track direction, and the Y axis forms a perpendicular right-hand coordinate frame with the X and Z axes. The unit vectors are denoted by $\boldsymbol{i}$, $\boldsymbol{j}$, and $\boldsymbol{k}$.

With frame $Cxyz$, the frame's origin is at the spacecraft position, the x axis points radially away from the Earth's center, the y axis points in the in-track direction with increasing true anomaly, and the z axis points in the cross-track direction. The unit vectors are denoted by $\boldsymbol{c}$, $\boldsymbol{d}$, and $\boldsymbol{k}$. This frame is denoted by $Axyz$ if its origin is at A and by $Bxyz$ if its origin is at B.

Subscripts 0 and 1 denote the initial orbit and the trajectory, respectively. Since the argument of perigee of the initial orbit, denoted by ω_0, is constant, the zero ω_0 case is investigated here to simplify the expressions. The results for the nonzero ω_0 case can be obtained via a simple coordinate transformation from the results for the zero ω_0 case. Thus, the relationships between unit vectors $\mathbf{c}$, $\mathbf{d}$, and $\mathbf{i}$, $\mathbf{j}$ are

$$\begin{cases} \boldsymbol{c} = \cos \upsilon_0 \boldsymbol{i} + \sin \upsilon_0 \boldsymbol{j} \\ \boldsymbol{d} = -\sin \upsilon_0 \boldsymbol{i} + \cos \upsilon_0 \boldsymbol{j} \end{cases} \tag{3}$$

where υ_0 is the true anomaly of the point of application.

As shown in Fig. 2, the initial orbit represented by the solid line and the trajectory represented by the broken line intersect each other at the point of application denoted by A. The argument of perigee of the trajectory is denoted by ω_1. B represents a point on the trajectory. The angle between the position vectors for point A and point B is denoted by θ. Analogously, the angle between the orbital planes of the trajectory and the initial orbit is denoted by Δi. All of the angular metrics are defined as counterclockwise positive.

The relationship between the initial velocity and the impulse vectors in frame $Axyz$ is depicted by Fig. 3. The included angle β, termed the flight-path angle, is the angle between the initial velocity $\boldsymbol{v}_0$ and the y axis. The angle between the impulse vector and its projection on the xy plane is denoted by γ, termed the impulse elevation. Analogously, the angle between the projection and the x axis is denoted by α, termed the impulse azimuth.

The position and velocity vectors of the point of application can be written in frame $Axyz$ as

$$\boldsymbol{r}_0 = r_0 \boldsymbol{c} \tag{4}$$

$$\boldsymbol{v}_0 = v_0(\sin \beta \boldsymbol{c} + \cos \beta \boldsymbol{d}) \tag{5}$$

The impulse vector can be written in frame $Axyz$ as

$$\Delta \boldsymbol{v} = \lambda(\cos \gamma \cos \alpha \boldsymbol{c} + \cos \gamma \sin \alpha \boldsymbol{d} + \sin \gamma \boldsymbol{k}) \tag{6}$$

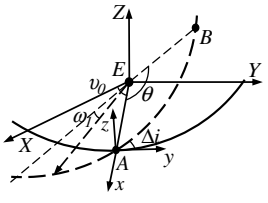

Fig. 2 Initial orbit and trajectory.

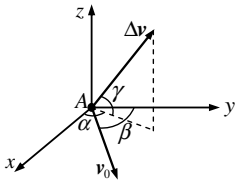

Fig. 3 Initial velocity and impulse vectors.

where λ is the magnitude of the impulse vector. It is well known that in Keplerian motion, the distance from the spacecraft to the Earth's center, r, and the magnitude of the velocity, v, are given by

$$r = \frac{p}{1 + e\cos\upsilon} \tag{7}$$

$$v = \sqrt{\frac{\mu(e^2 + 2e\cos\upsilon + 1)}{p}} \tag{8}$$

where p is the semilatus rectum of the orbit. The relationship between β and υ is

$$\tan\beta = \frac{e\sin\upsilon}{1 + e\cos\upsilon} \tag{9}$$

After the impulse is applied, the position vector for the point of application remains unchanged, but the velocity vector becomes

$$\boldsymbol{v}_1 = \boldsymbol{v}_0 + \Delta\boldsymbol{v} \tag{10}$$

Substituting Eqs. (3), (5), and (6) into Eq. (10) yields

$$\begin{aligned}\boldsymbol{v}_1 = {} & [v_0\sin(\beta - \upsilon_0) + \lambda\cos\gamma\cos(\alpha + \upsilon_0)]\boldsymbol{i} + [v_0\cos(\beta - \upsilon_0) \\ & + \lambda\cos\gamma\sin(\alpha + \upsilon_0)]\boldsymbol{j} + \lambda\sin\gamma\boldsymbol{k}\end{aligned} \tag{11}$$

The two fundamental vectors of the orbit, the angular momentum and the eccentricity vectors, can be written as

$$\boldsymbol{h} = \boldsymbol{r}\times\boldsymbol{v} \tag{12}$$

$$\boldsymbol{e} = \frac{\boldsymbol{v}\times\boldsymbol{h}}{\mu} - \frac{\boldsymbol{r}}{r} \tag{13}$$

Substituting Eqs. (3), (4), and (11) into Eqs. (12) and (13), then simplifying the resulting expressions gives the angular momentum and eccentricity vectors for the trajectory expressed in frame $EXYZ$:

$$\begin{aligned}\boldsymbol{h}_1 = {} & r_0\lambda\sin\upsilon_0\sin\gamma\boldsymbol{i} - r_0\lambda\cos\upsilon_0\sin\gamma\boldsymbol{j} \\ & + (h_0 + r_0\lambda\sin\alpha\cos\gamma)\boldsymbol{k}\end{aligned} \tag{14}$$

$$\boldsymbol{e}_1 = e_{1i}\boldsymbol{i} + e_{1j}\boldsymbol{j} + e_{1k}\boldsymbol{k} \tag{15}$$

where

$$\begin{aligned}e_{1i} = {} & \frac{h_0 + r_0\lambda\sin\alpha\cos\gamma}{\mu}[v_0\cos(\beta - \upsilon_0) + \lambda\cos\gamma\sin(\alpha + \upsilon_0)] \\ & + \frac{r_0\lambda^2\sin^2\gamma\cos\upsilon_0}{\mu} - \cos\upsilon_0 \\ e_{1j} = {} & -\frac{h_0 + r_0\lambda\cos\gamma\sin\alpha}{\mu}[v_0\sin(\beta - \upsilon_0) \\ & + \lambda\cos\gamma\cos(\alpha + \upsilon_0)] + \frac{r_0\lambda^2\sin^2\gamma\sin\upsilon_0}{\mu} - \sin\upsilon_0 \\ e_{1k} = {} & -\frac{r_0\lambda\sin\gamma}{\mu}(v_0\sin\beta + \lambda\cos\gamma\cos\alpha)\end{aligned}$$

From Eq. (15), the eccentricity magnitude of the trajectory is

$$\begin{aligned}e_1^2 = {} & 1 + [\lambda^2\sin^2\gamma + (\lambda\cos\gamma\sin\alpha + v_0\cos\beta)^2] \\ & \times\left[\frac{r_0^2}{\mu^2}(\lambda^2 + v_0^2 + 2\lambda v_0\cos\gamma\sin(\alpha + \beta)) - \frac{2r_0}{\mu}\right]\end{aligned} \tag{16}$$

The angle between the planes of the trajectory and the initial orbit satisfies

$$\cos\Delta i = \frac{\boldsymbol{h}_0\cdot\boldsymbol{h}_1}{h_0 h_1} \tag{17}$$

Substituting Eq. (14) into Eq. (17) yields

$$\cos\Delta i = \frac{h_0 + r_0\lambda\sin\alpha\cos\gamma}{\sqrt{r_0^2\lambda^2\sin^2\gamma + (h_0 + r_0\lambda\sin\alpha\cos\gamma)^2}} \tag{18}$$

The sine and cosine of the true anomaly υ are given by

$$\sin\upsilon = \frac{h}{\mu e r}\boldsymbol{r}\cdot\boldsymbol{v} \tag{19}$$

$$\cos\upsilon = \frac{\boldsymbol{r}\cdot\boldsymbol{e}}{re} \tag{20}$$

Substituting Eqs. (11), (14), and (15) into Eqs. (19) and (20) then simplifying the resulting expressions gives the sine and cosine of the true anomaly of the point of application on the trajectory as

$$\begin{aligned}\sin\upsilon = {} & \frac{v_0\sin\beta + \lambda\cos\gamma\cos\alpha}{\mu e_1} \\ & \times\sqrt{r_0^2\lambda^2\sin^2\gamma + (h_0 + r_0\lambda\sin\alpha\cos\gamma)^2}\end{aligned} \tag{21}$$

$$\cos\upsilon_1 = \frac{r_0}{\mu e_1}[(v_0\cos\beta + \lambda\cos\gamma\sin\alpha)^2 + \lambda^2\sin^2\gamma] - \frac{1}{e_1} \tag{22}$$

The semilatus rectum of the trajectory can be determined to be

$$p_1 = \frac{r_0^2\lambda^2\sin^2\gamma + (h_0 + r_0\lambda\sin\alpha\cos\gamma)^2}{\mu} \tag{23}$$

Let superscripts E and B denote vectors expressed in frames $EXYZ$ and $Bxyz$, and let subscript B denote point B. The position vector for point B on the trajectory in frame $Bxyz$ is given by

$$\boldsymbol{r}_B^B = \begin{bmatrix}\frac{p_1}{1 + e_1\cos(\theta + \upsilon_1)} \\ 0 \\ 0\end{bmatrix} \tag{24}$$

The rotation matrix transforming any vector in frame $Bxyz$ into frame $EXYZ$ can be characterized by an Euler 3-1-3 rotation. When the counterclockwise direction is considered as positive and the three Eulerian angles are $-\theta$, $-\Delta i$, and $-\upsilon_0$ in turn, the rotation matrix is

$$C_{EB} = C_z(-\upsilon_0)C_x(-\Delta i)C_z(-\theta) \tag{25}$$

where

$$C_z(-\upsilon_0) = \begin{bmatrix}\cos\upsilon_0 & -\sin\upsilon_0 & 0 \\ \sin\upsilon_0 & \cos\upsilon_0 & 0 \\ 0 & 0 & 1\end{bmatrix}$$

$$C_x(-\Delta i) = \begin{bmatrix}1 & 0 & 0 \\ 0 & \cos\Delta i & -\sin\Delta i \\ 0 & \sin\Delta i & \cos\Delta i\end{bmatrix}$$

$$C_z(-\theta) = \begin{bmatrix}\cos\theta & -\sin\theta & 0 \\ \sin\theta & \cos\theta & 0 \\ 0 & 0 & 1\end{bmatrix}$$

Hence, the position vector for point B can be written in frame $EXYZ$ as

$$\boldsymbol{r}_B^E = C_{EB}\begin{bmatrix} \frac{p_1}{1+e_1\cos(\theta+\upsilon_1)} \\ 0 \\ 0 \end{bmatrix} \tag{26}$$

Substituting Eq. (25) into Eq. (26) yields

$$\boldsymbol{r}_B^E = \begin{bmatrix} \cos\upsilon_0\cos\theta - \sin\upsilon_0\cos\Delta i\sin\theta \\ \sin\upsilon_0\cos\theta + \cos\upsilon_0\cos\Delta i\sin\theta \\ \sin\Delta i\sin\theta \end{bmatrix} \frac{p_1}{1+e_1\cos(\theta+\upsilon_1)} \tag{27}$$

This equation describes the trajectory generated by an arbitrary direction impulse applied at any point on the initial orbit. The equation is expressed in frame $EXYZ$ and the variables υ_0, α, and γ in Eq. (27) can vary over the interval $[0, 2\pi)$.

Especially, the necessary condition for the circular generated trajectory is the existence of a set of parameters υ_0, α, and γ satisfying $\boldsymbol{e}_1 = 0$, since the impulse magnitude is fixed, this exclusive situation rarely happens. Moreover, if this situation does exist, the three parameters can be obtained by setting $\boldsymbol{e}_1 = 0$, which means the generated trajectory is determined. Then the relationship between this circular generated trajectory and the boundary of the reachable domain can be analyzed.

Before deriving the reachable domain boundary, it is essential to emphasize that the points on the boundary are not related to the apogees/perigees of the trajectories. Although the apogee/perigee is the point on-orbit at which the spacecraft is furthest/closest to the Earth's center, the reachable domain boundary can be shown to be independent of the apogees/perigees of the trajectories. Especially, when the initial eccentricity is quite large, the apogees/perigees can be far from the boundary.

IV. Equations for the Ellipsoid of Revolution and the Plane Containing the Trajectory

An arbitrary direction impulse will change both the inclination and the longitude of the ascending node of the trajectory. Therefore, the trajectories form a family of curves in space. Consequently, the boundary of the reachable domain for this condition does not satisfy the envelope definition either for curves in a plane or for surfaces. However, the elliptical trajectory can be regarded as the intersection of a plane and an ellipsoid of revolution, and this concept is used here. This section presents the equations for the ellipsoid of revolution and the plane containing the trajectory in terms of υ_0, α, and γ.

A. Ellipsoid of Revolution Containing the Trajectory

The equation for the ellipsoid of revolution containing the trajectory can be described in terms of the angular momentum and eccentricity vectors as

$$\boldsymbol{e}\cdot\boldsymbol{R} = \frac{h^2}{\mu} - R \tag{28}$$

As shown in Fig. 4, in frame $EXYZ$, κ denotes the angle between the position vector $\boldsymbol{R}$ on the ellipsoid of revolution and its projection on the XY plane, termed the position elevation, and ι denotes the angle between the projection and the X axis, termed the position azimuth.

In frame $Exyz$, Eq. (28) can be written as

$$\begin{aligned} R &= f(\kappa, \iota, \upsilon_0, \alpha, \gamma) \\ &= \frac{p_1}{1 + e_{1i}\cos\kappa\cos\iota + e_{1j}\cos\kappa\sin\iota + e_{1k}\sin\kappa} \end{aligned} \tag{29}$$

On the ellipsoid-of-revolution equation $f(\kappa, \iota, \upsilon_0, \alpha, \gamma)$, κ and ι are variables, whereas υ_0, α, and γ are parameters.

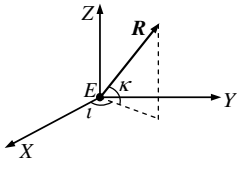

Fig. 4 Definition of the ellipsoid-of-revolution vector.

B. Plane Containing the Trajectory

The equation of the orbital plane, which is perpendicular to the angular momentum vector of the trajectory, can be written as

$$\boldsymbol{h}\cdot\boldsymbol{r} = 0 \tag{30}$$

Substituting Eq. (14) into Eq. (30) yields

$$\begin{aligned} g(x, y, z, \upsilon_0, \alpha, \gamma) &= \sin\upsilon_0\sin\gamma x - \cos\upsilon_0\sin\gamma y \\ &+ \left(\sqrt{\frac{\mu}{p_0}}\frac{1+e_0\cos\upsilon_0}{\lambda} + \sin\alpha\cos\gamma\right)z = 0 \end{aligned} \tag{31}$$

where x,y, and z are the components of $\boldsymbol{r}$ expressed in frame $EXYZ$. In the plane equation $g(x, y, z, \upsilon_0, \alpha, \gamma)$, x, y, and z are variables, whereas υ_0, α, and γ are parameters.

The following sections describe the envelopes of the ellipsoid-of-revolution family and the plane family for three scenarios. The actual reachable domain for spacecraft is contained in the torus formed by the intersection of these two envelopes, and this torus is defined as the upper bound on the actual reachable domain.

V. Arbitrary Point of Application and Fixed Impulse Direction

The effect of the point of application is analyzed first. Consider the scenario with a fixed direction impulse applied at any point on the initial orbit, which means that the parameter υ_0 varies over the interval $[0, 2\pi)$, whereas the other two parameters, α and γ, are constant. The envelopes of the ellipsoid-of-revolution family and the plane family for this scenario are given here.

A. Ellipsoid-of-Revolution-Family Envelope

From the surface-family envelope definition, both Eq. (29) and the following expression should be satisfied:

$$\frac{\partial f(\kappa, \iota, \upsilon_0)}{\partial\upsilon_0} = 0 \tag{32}$$

Equation (32) is equivalent to

$$\begin{aligned} &\left(\frac{\partial p_1}{\partial\upsilon_0}e_{1i} - p_1\frac{\partial e_{1i}}{\partial\upsilon_0}\right)\cos\kappa\cos\iota + \left(\frac{\partial p_1}{\partial\upsilon_0}e_{1j} - p_1\frac{\partial e_{1j}}{\partial\upsilon_0}\right)\cos\kappa\sin\iota \\ &+ \left(\frac{\partial p_1}{\partial\upsilon_0}e_{1k} - p_1\frac{\partial e_{1k}}{\partial\upsilon_0}\right)\sin\kappa + \frac{\partial p_1}{\partial\upsilon_0} = 0 \end{aligned} \tag{33}$$

where

$$\begin{aligned} \frac{\partial p_1}{\partial\upsilon_0} &= \frac{2p_0e_0\sin\upsilon_0}{\mu(1+e_0\cos\upsilon_0)^2}[r_0\lambda^2\sin^2\gamma \\ &+ (h_0 + r_0\lambda\sin\alpha\cos\gamma)\lambda\sin\alpha\cos\gamma] \\ \frac{\partial e_{1i}}{\partial\upsilon_0} &= \left[\lambda\cos\gamma\cos(\alpha+\upsilon_0) - \sqrt{\frac{\mu}{p_0}}\sin\upsilon_0\right]\frac{h_0 + r_0\lambda\sin\alpha\cos\gamma}{\mu} \\ &+ \frac{\lambda^2\sin^2\gamma}{\mu}\left[\frac{p_0e_0\sin\upsilon_0}{(1+e_0\cos\upsilon_0)^2} - \sin\upsilon_0\right] + \left[\sqrt{\frac{\mu}{p_0}}(e_0+\cos\upsilon_0)\right. \\ &\left. + \lambda\cos\gamma\sin(\alpha+\upsilon_0)\right]\frac{\lambda\sin\alpha\cos\gamma p_0e_0\sin\upsilon_0}{\mu(1+e_0\cos\upsilon_0)^2} + \sin\upsilon_0 \\ \frac{\partial e_{1j}}{\partial\upsilon_0} &= \left[\sqrt{\frac{\mu}{p_0}}\sin\upsilon_0 - \lambda\cos\gamma\cos(\alpha+\upsilon_0)\right]\frac{r_0e_0\lambda\cos\gamma\sin\alpha\sin\upsilon_0}{\mu(1+e_0\cos\upsilon_0)} \\ &- \cos\upsilon_0 + \left[\sqrt{\frac{\mu}{p_0}}\cos\upsilon_0 + \lambda\cos\gamma\sin(\alpha+\upsilon_0)\right] \\ &\times\frac{h_0 + r_0\lambda\cos\gamma\sin\alpha}{\mu} + \frac{\lambda^2\sin^2\gamma}{\mu}\left(\frac{p_0e_0\sin\upsilon_0}{(1+e_0\cos\upsilon_0)^2} + \cos\upsilon_0\right) \\ \frac{\partial e_{1k}}{\partial\upsilon_0} &= -\left(\sqrt{\frac{\mu}{p_0}}e_0\sin\upsilon_0 + \lambda\cos\gamma\cos\alpha\right)\frac{\lambda r_0e_0\sin\gamma\sin\upsilon_0}{\mu(1+e\cos\upsilon_0)} \\ &- \frac{\lambda r_0e_0\sin\gamma\cos\upsilon_0}{\sqrt{\mu p_0}} \end{aligned}$$

By replacing ι with s, Eq. (33) can be transformed from the trigonometric form into a parametric algebraic form as

$$(C_1 - A_1)s^2 + 2B_1 s + C_1 + A_1 = 0 \tag{34}$$

where

$$s = \tan\frac{\iota}{2} \qquad \iota \in [0, 2\pi)$$

$$A_1 = \left(\frac{\partial p_1}{\partial \upsilon_0} e_{1i} - p_1 \frac{\partial e_{1i}}{\partial \upsilon_0}\right)\cos\kappa$$

$$B_1 = \left(\frac{\partial p_1}{\partial \upsilon_0} e_{1j} - p_1 \frac{\partial e_{1j}}{\partial \upsilon_0}\right)\cos\kappa$$

$$C_1 = \left(\frac{\partial p_1}{\partial \upsilon_0} e_{1k} - p_1 \frac{\partial e_{1k}}{\partial \upsilon_0}\right)\sin\kappa + \frac{\partial p_1}{\partial \upsilon_0}$$

The parametric substitution method will be frequently used in this study, so its validity will be proved first. The interval of ι is $[0, 2\pi)$, and the mapping from ι to s is discontinuous only at the point $\iota = \pi$, which corresponds to the condition of $s = \infty$. Since s tends to $+\infty$ as ι tends to π^-, whereas s tends to $-\infty$ as ι tends to π^+, and both $\iota = \pi^+$ and $\iota = \pi^-$ correspond to the same equality for Eq. (34), which leads to the condition $C_1 = A_1$, $+\infty$ and $-\infty$ can be combined to one value ∞ to make the mapping continuous and one-to-one, where $0 \le |s| \le \infty$. As a result, Eq. (34) is equivalent to Eq. (33). The solutions of Eq. (34) are

$$\begin{cases} s_1 = \frac{-B_1 + \sqrt{B_1^2 - C_1^2 + A_1^2}}{C_1 - A_1} \\ s_2 = \frac{-B_1 - \sqrt{B_1^2 - C_1^2 + A_1^2}}{C_1 - A_1} \end{cases} \tag{35}$$

According to the definition of s, the desired angle ι is

$$\begin{cases} \iota_1 = 2\arctan s_1 \\ \iota_2 = 2\arctan s_2 \end{cases} \tag{36}$$

Substituting ι_1 and ι_2 in Eqs. (36) into Eq. (29) gives the envelope of the family of the ellipsoids of revolution containing the trajectories generated after a fixed direction impulse is applied at any point on the initial orbit.

B. Plane-Family Envelope

From the surface-family envelope definition, both Eq. (31) and the following expression should be satisfied:

$$\frac{\partial g(x, y, z, \upsilon_0)}{\partial \upsilon_0} = 0 \tag{37}$$

Equation (37) is equivalent to

$$\sin\gamma(e_0 + \cos\upsilon_0)x + \sin\gamma\sin\upsilon_0 y + e_0\sin\upsilon_0\sin\alpha\cos\gamma z = 0 \tag{38}$$

By replacing υ_0 with m, Eq. (38) can be transformed from the trigonometric form into a parametric algebraic form as

$$(e_0 - 1)x\sin\gamma m^2 + 2(e_0\sin\alpha\cos\gamma z + \sin\gamma y)m + (e_0 + 1)x\sin\gamma = 0 \tag{39}$$

where

$$m = \tan\frac{\upsilon_0}{2} \qquad \upsilon_0 \in [0, 2\pi)$$

The solutions of Eq. (39) can be written as

$$\begin{cases} m_1 = \frac{(e_0\sin\alpha c\tan\gamma z + y) + \sqrt{(e_0\sin\alpha c\tan\gamma z + y)^2 - (e_0^2 - 1)x^2}}{(1 - e_0)x} \\ m_2 = \frac{(e_0\sin\alpha c\tan\gamma z + y) - \sqrt{(e_0\sin\alpha c\tan\gamma z + y)^2 - (e_0^2 - 1)x^2}}{(1 - e_0)x} \end{cases} \tag{40}$$

The definition of m is used to get the desired true anomaly υ_0 as

$$\begin{cases} \upsilon_{01} = 2\arctan m_1 \\ \upsilon_{02} = 2\arctan m_2 \end{cases} \tag{41}$$

Substituting υ_{01} and υ_{02} in Eqs. (41) into Eq. (31) gives the envelope of the family of the planes containing the trajectories generated after a fixed direction impulse is applied at any point on the initial orbit:

$$\begin{cases} z_1 = \frac{\lambda\sqrt{p_0}[2m_1 x - (1 - m_1^2)y]\sin\gamma}{\sqrt{\mu}[1 + m_1^2 + (1 - m_1^2)e_0] + \lambda\sqrt{p_0}(1 + m_1^2)\sin\alpha\cos\gamma} \\ z_2 = \frac{\lambda\sqrt{p_0}[2m_2 x - (1 - m_2^2)y]\sin\gamma}{\sqrt{\mu}[1 + m_2^2 + (1 - m_2^2)e_0] + \lambda\sqrt{p_0}(1 + m_2^2)\sin\alpha\cos\gamma} \end{cases} \tag{42}$$

VI. Fixed Point of Application and Arbitrary Impulse Direction

The effect of impulse direction is analyzed. Consider the scenario with an arbitrary direction impulse applied at a fixed point on the initial orbit, which means that the parameters α and γ vary in the interval $[0, 2\pi)$, while the other parameter, υ_0, is constant. Maneuvering commands are usually executed at a specified instant, therefore, the point of application is fixed, which corresponds well to this scenario. The envelopes of the ellipsoid-of-revolution family and the plane family for this scenario are given here.

A. Ellipsoid-of-Revolution-Family Envelope

From the surface-family envelope definition, both Eq. (29) and the following expressions should be satisfied:

$$\begin{cases} \frac{\partial f(\kappa, \iota, \alpha, \gamma)}{\partial \alpha} = 0 \\ \frac{\partial f(\kappa, \iota, \alpha, \gamma)}{\partial \gamma} = 0 \end{cases} \tag{43}$$

Equations (43) are equivalent to

$$\begin{cases} (\frac{\partial p_1}{\partial \alpha} e_{1i} - p_1 \frac{\partial e_{1i}}{\partial \alpha})\cos\kappa\cos\iota + (\frac{\partial p_1}{\partial \alpha} e_{1j} - p_1 \frac{\partial e_{1j}}{\partial \alpha})\cos\kappa\sin\iota \\ \quad + (\frac{\partial p_1}{\partial \alpha} e_{1k} - p_1 \frac{\partial e_{1k}}{\partial \alpha})\sin\kappa + \frac{\partial p_1}{\partial \alpha} = 0 \\ (\frac{\partial p_1}{\partial \gamma} e_{1i} - p_1 \frac{\partial e_{1i}}{\partial \gamma})\cos\kappa\cos\iota + (\frac{\partial p_1}{\partial \gamma} e_{1j} - p_1 \frac{\partial e_{1j}}{\partial \gamma})\cos\kappa\sin\iota \\ \quad + (\frac{\partial p_1}{\partial \gamma} e_{1k} - p_1 \frac{\partial e_{1k}}{\partial \gamma})\sin\kappa + \frac{\partial p_1}{\partial \gamma} = 0 \end{cases} \tag{44}$$

where

$$\frac{\partial p_1}{\partial \alpha} = \frac{2r_0\lambda\cos\alpha\cos\gamma}{\mu}(h_0 + r_0\lambda\sin\alpha\cos\gamma)$$

$$\frac{\partial e_{1i}}{\partial \alpha} = \frac{h_0}{\mu}\lambda\cos\gamma\cos(\alpha + \upsilon_0) + (e_0 + \cos\upsilon_0)\frac{r_0\lambda\cos\gamma\cos\alpha}{\sqrt{\mu p_0}} + \frac{r_0\lambda^2\cos^2\gamma\sin(2\alpha + \upsilon_0)}{\mu}$$

$$\frac{\partial e_{1j}}{\partial \alpha} = \frac{h_0}{\mu}\lambda\cos\gamma\sin(\alpha + \upsilon_0) - \frac{r_0\lambda^2\cos^2\gamma}{\mu}\cos(2\alpha + \upsilon_0) + \frac{r_0\lambda\cos\gamma\cos\alpha\sin\upsilon_0}{\sqrt{\mu p_0}}$$

$$\frac{\partial e_{1k}}{\partial \alpha} = \frac{r_0\lambda^2\sin\gamma\cos\gamma\sin\alpha}{\mu}$$

$$\frac{\partial p_1}{\partial \gamma} = \frac{2r_0\lambda\sin\gamma}{\mu}(r_0\lambda\cos\gamma\cos^2\alpha - h_0\sin\alpha)$$

$$\frac{\partial e_{1i}}{\partial \gamma} = \frac{2r_0\lambda^2 \sin\gamma\cos\gamma[\cos\upsilon_0 - \sin(\alpha+\upsilon_0)\sin\alpha] - h_0\lambda\sin\gamma\sin(\alpha+\upsilon_0)}{\mu} - \frac{r_0\lambda\sin\alpha\sin\gamma}{\sqrt{\mu p_0}}(e_0+\cos\upsilon_0)$$

$$\frac{\partial e_{1j}}{\partial \gamma} = \frac{2r_0\lambda^2 \sin\gamma\cos\gamma[\sin\upsilon_0 + \sin\alpha\cos(\alpha+\upsilon_0)] + h_0\lambda\sin\gamma\cos(\alpha+\upsilon_0)}{\mu} - \frac{r_0\lambda\sin\gamma\sin\alpha\sin\upsilon_0}{\sqrt{\mu p_0}}$$

$$\frac{\partial e_{1k}}{\partial \gamma} = -\frac{r_0\lambda^2\cos\alpha\cos 2\gamma}{\mu} - \frac{r_0\lambda e\cos\gamma\sin\upsilon_0}{\sqrt{\mu p_0}}$$

Using $s = \tan\frac{\iota}{2}$, Eqs. (44) can be rewritten in the following forms:

$$\begin{cases} (C_2 - A_2)s^2 + 2B_2 s + C_2 + A_2 = 0 \\ (C_3 - A_3)s^2 + 2B_3 s + C_3 + A_3 = 0 \end{cases} \tag{45}$$

where

$$A_2 = \left(\frac{\partial p_1}{\partial\alpha}e_{1i} - p_1\frac{\partial e_{1i}}{\partial\alpha}\right)\cos\kappa$$

$$B_2 = \left(\frac{\partial p_1}{\partial\alpha}e_{1j} - p_1\frac{\partial e_{1j}}{\partial\alpha}\right)\cos\kappa$$

$$C_2 = \left(\frac{\partial p_1}{\partial\alpha}e_{1k} - p_1\frac{\partial e_{1k}}{\partial\alpha}\right)\sin\kappa + \frac{\partial p_1}{\partial\alpha}$$

$$A_3 = \left(\frac{\partial p_1}{\partial\gamma}e_{1i} - p_1\frac{\partial e_{1i}}{\partial\gamma}\right)\cos\kappa$$

$$B_3 = \left(\frac{\partial p_1}{\partial\gamma}e_{1j} - p_1\frac{\partial e_{1j}}{\partial\gamma}\right)\cos\kappa$$

$$C_3 = \left(\frac{\partial p_1}{\partial\gamma}e_{1k} - p_1\frac{\partial e_{1k}}{\partial\gamma}\right)\sin\kappa + \frac{\partial p_1}{\partial\gamma}$$

The relationship between α and γ can be derived from Eqs. (45). This relationship along with $\iota = 2\arctan s$ can be substituted into Eq. (29) to obtain the envelope of the family of the ellipsoids of revolution containing the trajectories generated after an arbitrary direction impulse is applied at a fixed point on the initial orbit. The relationship between α and γ is very complicated and can not be given by an explicit formula; therefore, the ellipsoid-of-revolution-family envelope must be obtained by numerically solving the nonlinear equations.

B. Plane-Family Range

In this scenario, all the planes containing the trajectories cover the Earth's center and the point of application, so they form a pencil of planes. From the plane-family envelope definition, the line crossing the Earth's center and the point of application is an envelope, however, this envelope is not sufficient to describe the distribution of the reachable domain along the angular momentum vector of the initial orbit. Therefore, the distribution is found by analyzing the parameters in the equations based on the envelope definition.

From the surface-family envelope definition, both Eq. (31) and the following expressions should be satisfied:

$$\begin{cases} \frac{\partial g(x,y,z,\alpha,\gamma)}{\partial\alpha} = 0 \\ \frac{\partial g(x,y,z,\alpha,\gamma)}{\partial\gamma} = 0 \end{cases} \tag{46}$$

Equations (46) are equivalent to

$$\begin{cases} \cos\alpha\cos\gamma z = 0 \\ \sin\upsilon_0\cos\gamma x - \cos\upsilon_0\cos\gamma y - \sin\alpha\sin\gamma z = 0 \end{cases} \tag{47}$$

At $z = 0$, Eqs. (47) correspond to the line crossing the Earth's center and the point of application, which is the envelope of the pencil of planes satisfying the definition. Another solution of Eqs. (47), $\cos\gamma = 0$, means that the impulse is perpendicular to the initial orbital plane. Since the perpendicular impulse will cause the maximum rotation of the initial plane, this is the condition for the range of the plane family. At the same time, the expression $\sin\alpha = 0$ is also automatically satisfied. In addition, the envelope solution obtained for $z = 0$ is also covered by the range of the plane family obtained for $\cos\gamma = 0$. Analysis of the equations show that the third possibility of $\cos\alpha = 0$ can be excluded.

Equations (31) and (47) can then be solved by transforming the trigonometric forms into parametric algebraic forms. The range of the family of the planes containing the trajectories could be obtained for an arbitrary direction impulse applied at a fixed point on the initial orbit:

$$\begin{cases} z_1 = \sqrt{\frac{p_0}{\mu}}\frac{\lambda(\sin\upsilon_0 x - \cos\upsilon_0 y)}{1+e_0\cos\upsilon_0} \\ z_2 = -\sqrt{\frac{p_0}{\mu}}\frac{\lambda(\sin\upsilon_0 x - \cos\upsilon_0 y)}{1+e_0\cos\upsilon_0} \end{cases} \tag{48}$$

VII. Arbitrary Point of Application and Impulse Direction

As mentioned earlier, the safe distance between spacecraft must be evaluated to avoid collisions caused by operating errors. Since the time and impulse direction of the error can not be forecasted, this section considers an arbitrary direction impulse applied at any point on the initial orbit, so that all three parameters (α, γ, and υ_0) vary in the interval $[0, 2\pi)$. The envelopes of the ellipsoid-of-revolution family and the plane family for this scenario are given here.

A. Ellipsoid-of-Revolution-Family Envelope

From the surface-family envelope definition, both Eq. (29) and the following expressions should be satisfied:

$$\begin{cases} \frac{\partial f(\kappa,\iota,\upsilon_0,\alpha,\gamma)}{\partial\upsilon_0} = 0 \\ \frac{\partial f(\kappa,\iota,\upsilon_0,\alpha,\gamma)}{\partial\alpha} = 0 \\ \frac{\partial f(\kappa,\iota,\upsilon_0,\alpha,\gamma)}{\partial\gamma} = 0 \end{cases} \tag{49}$$

Equations (49) are equivalent to

$$\begin{cases} \left(\frac{\partial p_1}{\partial\upsilon_0}e_{1i} - p_1\frac{\partial e_{1i}}{\partial\upsilon_0}\right)\cos\kappa\cos\iota + \left(\frac{\partial p_1}{\partial\upsilon_0}e_{1j} - p_1\frac{\partial e_{1j}}{\partial\upsilon_0}\right)\cos\kappa\sin\iota + \left(\frac{\partial p_1}{\partial\upsilon_0}e_{1k} - p_1\frac{\partial e_{1k}}{\partial\upsilon_0}\right)\sin\kappa + \frac{\partial p_1}{\partial\upsilon_0} = 0 \\ \left(\frac{\partial p_1}{\partial\alpha}e_{1i} - p_1\frac{\partial e_{1i}}{\partial\alpha}\right)\cos\kappa\cos\iota + \left(\frac{\partial p_1}{\partial\alpha}e_{1j} - p_1\frac{\partial e_{1j}}{\partial\alpha}\right)\cos\kappa\sin\iota + \left(\frac{\partial p_1}{\partial\alpha}e_{1k} - p_1\frac{\partial e_{1k}}{\partial\alpha}\right)\sin\kappa + \frac{\partial p_1}{\partial\alpha} = 0 \\ \left(\frac{\partial p_1}{\partial\gamma}e_{1i} - p_1\frac{\partial e_{1i}}{\partial\gamma}\right)\cos\kappa\cos\iota + \left(\frac{\partial p_1}{\partial\gamma}e_{1j} - p_1\frac{\partial e_{1j}}{\partial\gamma}\right)\cos\kappa\sin\iota + \left(\frac{\partial p_1}{\partial\gamma}e_{1k} - p_1\frac{\partial e_{1k}}{\partial\gamma}\right)\sin\kappa + \frac{\partial p_1}{\partial\gamma} = 0 \end{cases} \tag{50}$$

Once again, using $s = \tan\frac{\iota}{2}$, Eqs. (50) are rewritten as

$$\begin{cases} (C_1 - A_1)s^2 + 2B_1 s + C_1 + A_1 = 0 \\ (C_2 - A_2)s^2 + 2B_2 s + C_2 + A_2 = 0 \\ (C_3 - A_3)s^2 + 2B_3 s + C_3 + A_3 = 0 \end{cases} \tag{51}$$

The relationships between υ_0, α, and γ can be derived from Eqs. (51). These relationships along with $\iota = 2\arctan s$ are substituted into Eq. (29) to obtain the envelope of the family of the ellipsoids of revolution containing the trajectories generated after an arbitrary direction impulse is applied at any point on the initial orbit. Again, the ellipsoid-of-revolution-family envelope is obtained by numerically solving the nonlinear equations.

B. Plane-Family Envelope

From the surface-family envelope definition, both Eq. (31) and the following expressions should be satisfied:

$$\begin{cases} \frac{\partial g(x,y,z,\upsilon_0,\alpha,\gamma)}{\partial \upsilon_0} = 0 \\ \frac{\partial g(x,y,z,\upsilon_0,\alpha,\gamma)}{\partial \alpha} = 0 \\ \frac{\partial g(x,y,z,\upsilon_0,\alpha,\gamma)}{\partial \gamma} = 0 \end{cases} \tag{52}$$

Equations (52) are equivalent to

$$\begin{cases} \sin\gamma(e_0 + \cos\upsilon_0)x + \sin\gamma\sin\upsilon_0 y + e_0\sin\upsilon_0\sin\alpha\cos\gamma z = 0 \\ \cos\alpha\cos\gamma z = 0 \\ \sin\upsilon_0\cos\gamma x - \cos\upsilon_0\cos\gamma y - \sin\alpha\sin\gamma z = 0 \end{cases} \tag{53}$$

As mentioned earlier, $\cos\gamma = 0$ and $\sin\alpha = 0$ means that the impulse is perpendicular to the initial orbital plane, which is the condition for the plane-family envelope. Therefore, Eqs. (31) and (53) should be rewritten as

$$\begin{cases} (e_0 + \cos\upsilon_0)x + \sin\upsilon_0 y = 0 \\ \sin\gamma(\sin\upsilon_0 x - \cos\upsilon_0 y) + \sqrt{\frac{\mu}{p_0}}\frac{1+e_0\cos\upsilon_0}{\lambda} z = 0 \end{cases} \tag{54}$$

Once again, Eqs. (54) are solved by transforming the trigonometric forms into parametric algebraic forms to obtain the envelope of the family of the planes containing the trajectories generated after an arbitrary direction impulse is applied at any point on the initial orbit:

$$\begin{cases} z_1 = \sqrt{\frac{p_0}{\mu}}\frac{\lambda[(1-n_1^2)y - 2n_1 x]}{1+n_1^2+(1-n_1^2)e_0} \\ z_2 = -\sqrt{\frac{p_0}{\mu}}\frac{\lambda[(1-n_1^2)y - 2n_1 x]}{1+n_1^2+(1-n_1^2)e_0} \\ z_3 = \sqrt{\frac{p_0}{\mu}}\frac{\lambda[(1-n_2^2)y - 2n_2 x]}{1+n_2^2+(1-n_2^2)e_0} \\ z_4 = -\sqrt{\frac{p_0}{\mu}}\frac{\lambda[(1-n_2^2)y - 2n_2 x]}{1+n_2^2+(1-n_2^2)e_0} \end{cases} \tag{55}$$

where

$$\begin{cases} n_1 = \frac{y + \sqrt{y^2 - (e_0^2-1)x^2}}{(1-e_0)x} \\ n_2 = \frac{y - \sqrt{y^2 - (e_0^2-1)x^2}}{(1-e_0)x} \end{cases}$$

Equations (55) describe four ruled surfaces, but only a part of each surface belongs to the desired envelope, as can be determined by analyzing and restricting the scopes of x and y.

C. Special Scenario for a Circular Initial Orbit

This analysis has shown the difficulty of using simple formulae to describe the reachable domain for the spacecraft in an initial elliptical orbit, especially, when the initial eccentricity is large. However, the reachable domain can be more easily described for the spacecraft in an initial circular orbit due to the symmetry of a circle. In this case, the reachable domain is enveloped by two homocentric circles on each section in parallel with the initial orbital plane, and it reduces to a circle on the two symmetrical sections furthest from the initial orbital plane.

The largest and smallest radii of the envelope circles both occur when the section is identical to the initial orbital plane. The maximum distance from the spacecraft to Earth, which occurs with a tangential impulse, is

$$l_{\max} = \frac{\mu + r_0\lambda^2 + 2\lambda\sqrt{\mu r_0}}{\mu - r_0\lambda^2 - 2\lambda\sqrt{\mu r_0}}\, r_0 \tag{56}$$

where r_0 is the initial orbital radius. Similarly, the minimum distance from the spacecraft to Earth, which occurs when an impulse is applied directly opposite to the initial velocity, is

$$l_{\min} = \frac{\mu + r_0\lambda^2 - 2\lambda\sqrt{\mu r_0}}{\mu - r_0\lambda^2 + 2\lambda\sqrt{\mu r_0}}\, r_0 \tag{57}$$

When the initial eccentricity is equal to zero, Eqs. (55) reduce to the simpler form:

$$\begin{cases} z_1 = \sqrt{\frac{p_0}{\mu}}\lambda\sqrt{x^2 + y^2} \\ z_2 = -\sqrt{\frac{p_0}{\mu}}\lambda\sqrt{x^2 + y^2} \end{cases} \tag{58}$$

Equations (58) show the relationship between the height and radius of the circle representing the part of the reachable domain furthest from the initial orbital plane.

VIII. Numerical Simulation

Numerical simulations were conducted for an initial orbit having a semimajor axis of 16378.137 km and eccentricity of 0.5, and the impulse magnitude is 0.2 km/s.

For the first scenario, the true anomaly of the point of application is arbitrary, whereas the impulse azimuth and elevation are set to $\alpha = 20$ deg and $\gamma = 50$ deg. For the second scenario, the impulse azimuth and elevation are arbitrary, whereas the true anomaly of the point of application is set to $\upsilon_0 = 10$ deg. For the third scenario, both the point of application and the impulse direction are arbitrary.

The reachable domain for the spacecraft and the plane-family envelope in these three scenarios are depicted by Figs. 5–7. In each figure, the fuscous domain formed by solid lines represents the reachable domain and the shaded surface represents the plane-family envelope. The plane-family envelope includes several ruled surfaces (two for the first two scenarios and four for the third scenario), but only parts of the envelope are shown to express the relationships. These figures show that in each scenario the plane-family envelope accurately describes the distribution of the reachable domain along the angular momentum vector of the initial orbit.

The ellipsoid-of-revolution-family envelope in each scenario includes two closed surfaces. Since the angle between the planes of the trajectory and the initial orbit is rather small, less than 4.1 deg in all three scenarios, only the narrow region near the initial plane is of interest. The reachable domain for the spacecraft and the parts of the ellipsoid-of-revolution-family envelopes in these three scenarios are depicted by Figs. 8–10. In each figure, the fuscous domain formed by

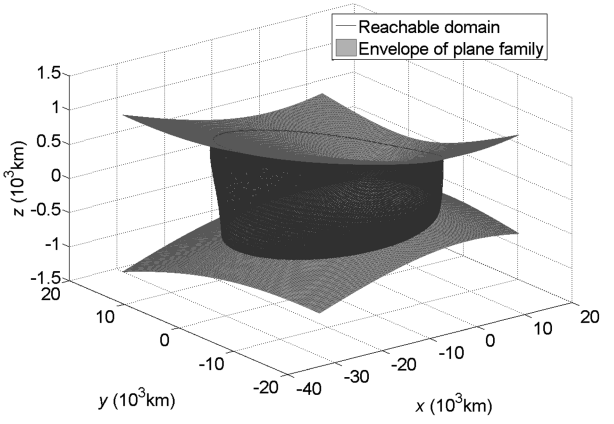

Fig. 5 Reachable domain and the plane-family envelope for arbitrary point of application.

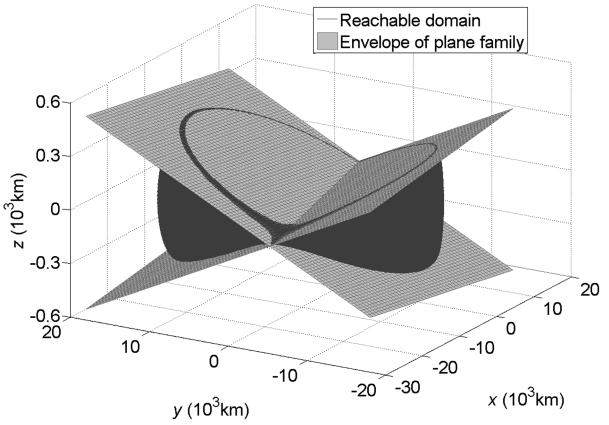

Fig. 6 Reachable domain and the plane-family envelope for arbitrary impulse direction.

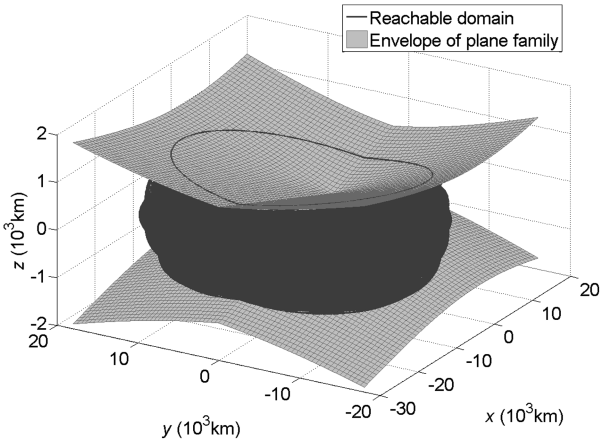

Fig. 7 Reachable domain and the plane-family envelope for arbitrary point of application and impulse direction.

the solid line represents the reachable domain and the surfaces formed by the symbol o represent the ellipsoid-of-revolution-family envelope. These figures show that in each scenario the reachable domain boundary is not identical to the ellipsoid-of-revolution-family envelope, but the envelope includes the whole reachable domain.

To visualize the result distinctly, the plane-family envelope and the ellipsoid-of-revolution-family envelope for arbitrary point of application and impulse direction are depicted by Figs. 11, in which the meanings of the symbols are the same with the anterior definition. The intersection of the envelopes is the conservative region given by

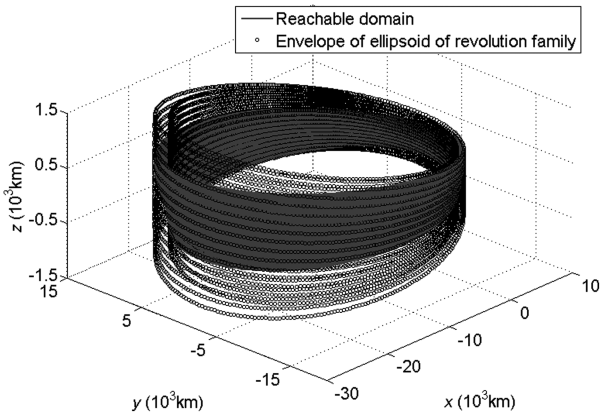

Fig. 8 Reachable domain and the ellipsoid-of-revolution-family envelope for arbitrary point of application.

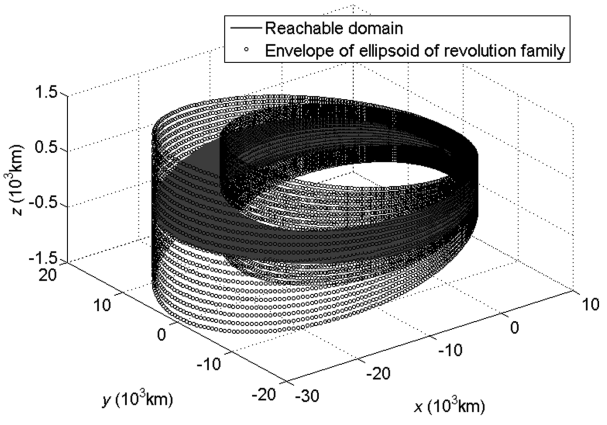

Fig. 9 Reachable domain and the ellipsoid-of-revolution-family envelope for arbitrary impulse direction.

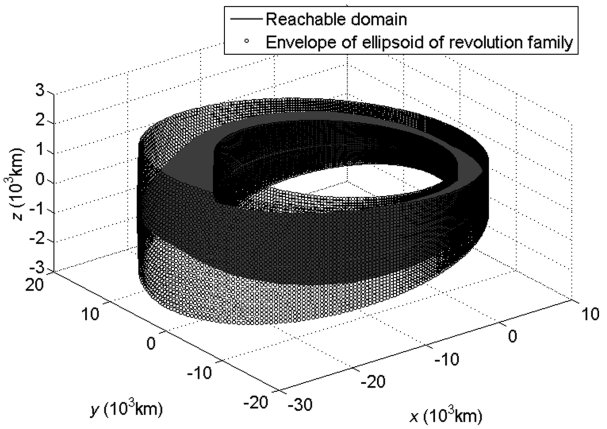

Fig. 10 Reachable domain and the ellipsoid-of-revolution-family envelope for arbitrary point of application and impulse direction.

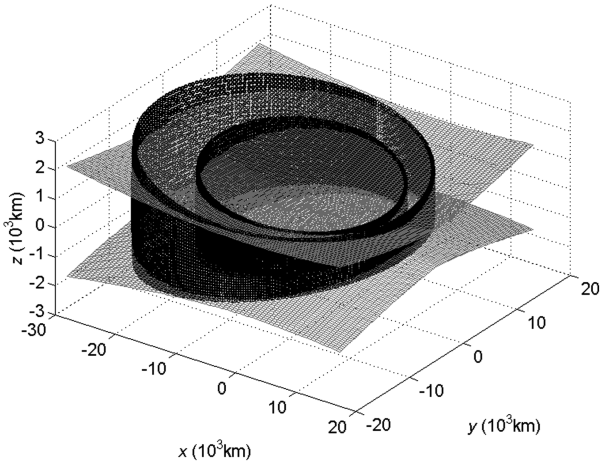

Fig. 11 Intersection of the plane-family envelope and the ellipsoid-of-revolution-family envelope for arbitrary point of application and impulse direction.

this method, which can be regarded as the upper bound on the actual reachable domain.

IX. Conclusions

The reachable domain for spacecraft was derived for a single fixed-magnitude impulse. Three typical scenarios were analyzed

with either of the point of application or the impulse direction being arbitrary or both being arbitrary.

First, the angular momentum and eccentricity vectors of the trajectory were derived, and the trajectory was given with no restriction on the eccentricity of the initial elliptical orbit.

Second, the reachable domain for spacecraft was analyzed for the three scenarios, based on the concept that an ellipse is the intersection of a plane and an ellipsoid of revolution. The equations for the ellipsoid of revolution and the plane containing the trajectories were used to determine the envelopes of the ellipsoid-of-revolution family and the plane family. The intersection of these two envelopes, which is reasonably close to the actual boundary, was defined as the upper bound on the actual reachable domain. When evaluating the safe distance between spacecraft, the region that is slightly larger than the actual reachable domain is more conservative.

As for the coplanar impulse case, the exact boundary of the reachable domain could be obtained since it satisfies the envelope definition of the curve family in a plane, which is a special application of the method given here.

Acknowledgments

The authors would like to acknowledge David M. Christopher, Tsinghua University, for the meticulous revision of the paper. This work was supported by the National Natural Science Foundation of China (no. 10832004) and the China Postdoctoral Science Foundation (no. 20080430417).

References

[1] Hoskins, A. B., and Atkins, E. M., "Satellite Formation Mission Optimization with a Multi-Impulse Design," *Journal of Spacecraft and Rockets*, Vol. 44, No. 2, 2007, pp. 425–433. doi:10.2514/1.19984

[2] Luo, Y. Z., Tang, G. J., Lei, Y. J., and Li, H. Y., "Optimization of Multiple-Impulse, Multiple-Revolution, Rendezvous-Phasing Maneuvers," *Journal of Guidance, Control, and Dynamics*, Vol. 30, No. 4, 2007, pp. 946–952. doi:10.2514/1.25620

[3] Long, A. M., Richards, M. G., and Hastings, D. E., "On-Orbit Servicing: A New Value Proposition for Satellite Design and Operation," *Journal of Spacecraft and Rockets*, Vol. 44, No. 4, 2007, pp. 964–976. doi:10.2514/1.27117

[4] Sidi, M. J., *Spacecraft Dynamics and Control*, Cambridge Univ. Press, New York, 1997, pp. 64–71, Chap. 3.

[5] Kamel, O. M., and Soliman, A. S., "On the Optimization of the Generalized Coplanar Hohmann Impulsive Transfer Adopting Energy Change Concept," *Acta Astronautica*, Vol. 56, No. 4, 2005, pp. 431–438. doi:10.1016/j.actaastro.2004.04.016

[6] Ranieri, C. L., "Path-Constrained Trajectory Optimization for Proximity Operations," AIAA/AAS Astrodynamics Specialist Conference and Exhibit, AIAA Paper 2008-6275, Honolulu, HI, August 2008.

[7] Richards, A., Schouwenaars, T., How, J. P., and Feron, E., "Spacecraft Trajectory Planning with Avoidance Constraints Using Mixed-Integer Linear Programming," *Journal of Guidance, Control, and Dynamics*, Vol. 25, No. 4, 2002, pp. 755–764. doi:10.2514/2.4943

[8] Roger, A. B., and McInnes, C. R., "Safety Constrained Free-Flyer Path Planning at the International Space Station," *Journal of Guidance, Control, and Dynamics*, Vol. 23, No. 6, 2000, pp. 971–979. doi:10.2514/2.4656

[9] Breger, L., and How, J. P., "Safe Trajectories for Autonomous Rendezvous of Spacecraft," *Journal of Guidance, Control, and Dynamics*, Vol. 31, No. 5, 2008, pp. 1478–1489. doi:10.2514/1.29590

[10] Vinh, N. X., Gilbert, E. G., Howe, R. M., Sheu, D. L., and Lu, P., "Reachable Domain for Interception at Hyperbolic Speeds," *Acta Astronautica*, Vol. 35, No. 1, 1995, pp. 1–8. doi:10.1016/0094-5765(94)00132-6

[11] Battin, R. H., *An Introduction to the Mathematics and Methods of Astro Dynamics*, AIAA, Reston, VA, 1999, pp. 516–517, Chap. 11.

[12] Gobetz, F. W., and Doll, J. R., "A Survey of Impulsive Trajectories," *AIAA Journal*, Vol. 7, No. 5, 1969, pp. 801–834. doi:10.2514/3.5231

[13] Spivak, M., *A Comprehensive Introduction to Differential Geometry*, Vol. 3, 2nd ed., Publish or Perish, Berkeley, CA, 1979, pp. 255–263, Chap. 3.